

A novel temperature parametric method for rapid maximum power point detection in photovoltaic modules

Soufyane Ait El Ouahab¹, Firdaous Bakkali¹, Abdellah Amghar¹, Rachid Zriouile², Hassan Sahsah¹, Meriem Boudouane²

¹Metrology and Information Processing Lab, Department of Physics, Faculty of Science Agadir, Ibn Zohr University, Agadir, Morocco

²Materials and Renewable Energy Lab, Ibn Zohr University, Agadir, Morocco

Article Info

Article history:

Received Sep 18, 2024

Revised Mar 31, 2025

Accepted May 6, 2025

Keywords:

Hill climbing

Maximum power point tracking

Photovoltaic

PI controller

Temperature parametric

ABSTRACT

Photovoltaic systems (PVS) exhibit variability in their maximum power point (MPP) output due to variations in irradiance and cell temperature. This can lead to reduced efficiency, as maximum power point tracking (MPPT) algorithms often have slow response times and limited ability to adapt to rapidly changing environmental conditions. New algorithms are therefore needed to capture more energy and improve the efficiency of these systems. In this context, this article presents a new method for temperature parametric (TP) and its implementation using a digital PI controller, a buck converter, and MATLAB-Simulink. This innovative approach relies on detecting the MPP by continuously measuring the cell temperature of the PV panel (T_{cell}) and solar irradiance (S). A 3D linear regression model connects these two parameters with the maximum current (I_{mpp}), enabling real-time monitoring of the MPP. We have applied this new method on two different types of PV (POLY-40W and BPSX330J) under a range of environmental conditions, including stable and dynamic scenarios. The results of the simulation demonstrate the superiority of our approach compared to the hill climbing (HC) for perturbation steps of HC (1%) and HC (2%). Our method achieves faster convergence time 0.009 s and high MPPT efficiency at 98.18%, fewer steady-state oscillations, and better detection.

This is an open access article under the [CC BY-SA](#) license.



Corresponding Author:

Soufyane Ait El Ouahab

Metrology and Information Processing Lab, Department of Physics, Faculty of Science Agadir

Ibn Zohr University

Agadir 80000, Morocco

Email: soufyane.aitelouahab@edu.uiz.ac.ma

1. INTRODUCTION

In recent times, there has been a global shift toward renewable energies driven by demographic, social, and industrial growth, as well as concerns about the greenhouse effect and the release of carbon dioxide [1]. This trend has spurred a multitude of innovations in the renewable energy sector. These technological advances embrace transformative strategies, concentrating on the establishment of more sustainable ecosystems. This initiative begins with the harnessing of solar energy, advancements in energy storage [2], and application in electric vehicles and heating systems [3], [4]. Although current solar technologies boast numerous advantages, there are still certain weaknesses and drawbacks, including intermittency in electricity production, performance drops under specific conditions, and non-linearity in the P-V characteristic. To enhance the efficiency of solar energy, researchers continually strive to operate photovoltaic generators (PVG) at maximum power to optimize their utilization while concurrently reducing costs and expenses related to photovoltaic systems (PVS) and equipment. This objective necessitates the

implementation of a DC-DC converter, facilitating the connection between the PVG and the receiver by compelling the generator to deliver its maximum power (MPPT) through algorithms.

In the literature, algorithms designed for uniform temperature and sunlight conditions can be categorized into three groups. The first category relies on introducing a disturbance to one of the parameters (duty cycle, voltage, or current) and subsequently measuring power to determine the direction of steps. Examples include incremental conductance [5], perturb and observe [6], and hill climbing HC [7]. Unfortunately, this category frequently encounters issues with convergence times and oscillations around the MPP, failing to strike a balance between these two factors. Specifically, increasing the perturbation step reduces the time needed to reach the MPP but also increases oscillations in steady-state operation, and vice versa. In both scenarios, this results in diminished system performance in terms of power output.

The second category involves algorithms dependent on iterations and the evolution of variables, such as particle swarm optimization (PSO) [8], firefly algorithm (FA) [9], artificial bee colony (ABC) [10], grey wolf optimization (GWO) [11], herd horse optimization (HHO) [12], differential evolution (DE) [13], cuckoo search (CS) [14], and bonobo optimizer [15]. Although this category offers notable advantages in terms of efficiency and faster convergence compared to the previous category, it also has some drawbacks. These include challenges in tuning coefficients, increased algorithm complexity, the need for substantial storage capacity, and significant oscillations under dynamically changing meteorological conditions.

The third category seeks to establish a connection between diverse parameters, enabling the swift and uncomplicated real-time prediction of the MPP without the need for extensive memory space for implementation. Table 1 (see Appendix) presents a timeline of various studies in this category [16]-[18] along with the corresponding mathematical models, as shown in (1)-(3). It describes the importance and contributions of our work in relation to relevant previous studies, and also lists the comparators, including the types of converters used, decision variables, linearity equations, discussion, remarks, results obtained, as well as the issues and challenges addressed.

The primary contributions of this article can be encapsulated as: i) Introducing a novel, straightforward, and effective MPPT control method based on three-dimensional linear regression employing a buck converter with PI controller; ii) Achieve minimal oscillation around the MPP, faster response times with minimal power losses, and lower complexity with a more straightforward approach; iii) Enhancement of the robustness of the proposed MPPT control algorithm to sudden, static, and dynamic fluctuations in solar irradiation and temperature; and iv) Carry out a comparative study between the proposed control method and the HC method. Our paper is structured in five sections. After this introduction, section 2 focuses on the modeling of the PV system, encompassing the PV panel, the DC-DC buck converter, and the PI controller. Section 3 presents two approaches for the MPPT (HC and the new technique proposed by temperature parametric (TP)). Then, section 4 details the simulation results. Finally, we conclude in section 5.

2. MPPT PHOTOVOLTAIC SYSTEMS (PVS)

Figure 1 depicts the PVS utilized in this study, consisting of key components such as the PV modules (PVM), the load, a PI controller, and a buck DC-DC converter controlled by an MPPT controller with integrated monitoring techniques. The converter works in conjunction with the PVM and resistive load to maximize power extraction. A pulse width modulation (PWM) signal generator adjusts the converter's duty cycle based on the PI controller's evaluation, which considers the difference between the current estimated by the MPPT controller and the actual current at the PV terminal [19]. The subsequent sections will provide a detailed analysis of each part of the system.

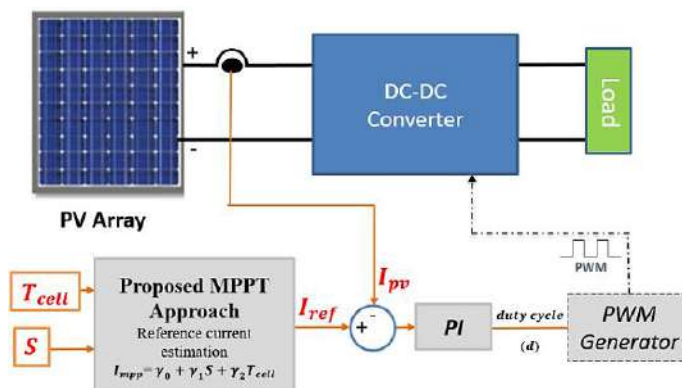


Figure 1. Proposed PVS

2.1. PI controller

PV systems generally share a common structure, with differentiation primarily based on the type of controller responsible for adjusting the duty cycle. In our study, we used an indirect controller for the proposed method (TP), employing a PI controller to adjust the duty cycle of the converter based on the disparity between I_{mpp} and I_{ref} . The PI controllers consist of a proportional term that corrects the current error, and an integral term that helps eliminate steady-state errors [20]. Table 2 presents the parameters of the PI controller used in this study.

Table 2. PI controller parameters

Parameter	P	I
Value	0.01	300

2.2. Characteristics of PVM

Figure 2 presents the equivalent circuit diagram of a single-diode (SD) PV module. The set of algebraic equations is derived based on Kirchhoff's laws, considering the characteristic behavior of all circuit elements, along with the Shockley equation that describes the diode's current. The mathematical model for the current-voltage characteristic is given by (4) [21].

$$I = I_{pv} - I_s \times \exp\left(\frac{(V + R_s \times I)}{A \times V_{th}} - 1\right) - (V + R_s \times I)/R_p \quad (4)$$

Where V_{th} : thermal voltage $V_{th} = (k \times T \times N_s)/q$; k , T , N_s , and q : Boltzmann constant, ambient temperature in K number of cells in series, and the electron charge.

2.3. Creating a model for the buck converter DC-DC

2.3.1. Principle

A buck converter is a DC-DC converter designed to reduce a higher DC voltage to a lower voltage. This relationship is given by (5) [22].

$$V_s = d \cdot V_e \quad (5)$$

Where $d = \frac{t_{on}}{T}$ is the ratio of time the switching element is ON (t_{on}) versus the switching oscillatory cycle T . It finds application in power supplies for electronic devices [23], battery chargers [24], and renewable energy systems [25]. Its reputation lies in its simplicity, high efficiency, and capacity to decrease voltage levels.

Figure 3 represents a brief explanation of how a buck converter works. Where (V_e) is the highest input voltage supplied to the converter. A switch (K) quickly turns the input voltage on and off. An inductor (L) is used to store energy during the on state of the switch. A diode (D) allows current to flow when the switch is off, thereby directing the energy stored in the inductor to the output. C_e and C_s are the input and output capacitors and are used to smooth the input and output voltage, respectively.

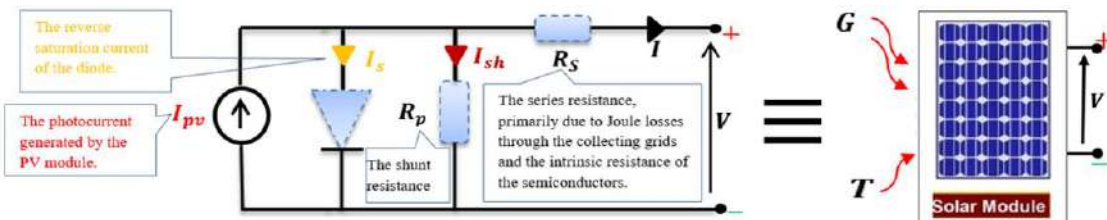


Figure 2. The SD model's equivalent circuit for the PVM

2.3.2. Theoretical study in continuous conduction mode (CCM)

The converter's functioning in a desired mode theoretical study in continuous conduction mode (CCM) or discontinuous conduction mode (DCM) is determined by the inductor current, and its elements must be crafted in a particular manner. To attain the designated inductance and capacitance values, the

steady-state equations of the converter need to be resolved in every subinterval of the switching period [26]. Switch On: ($0 < t < dT$) switch K is in the closed position, while D is in the blocked state.

$$V_e - V_s = L \times \frac{di_L}{dt} \Leftrightarrow i_L(t) = I_{L,min} + \frac{V_e - V_s}{L} t \quad (6)$$

At $t = dT$, the inductor current achieves its peak value:

$$I_{L,max} = I_{L,min} + \frac{V_e - V_s}{L} dT \quad (7)$$

Switch off: ($dT < t < T$) At $t = dT$, switch K is opened. Diode becomes conductive.

$$-V_s = L \times \frac{di_L}{dt} \Leftrightarrow i_L(t) = I_{L,max} - \frac{V_s}{L}(t - dT) \quad (8)$$

At $t = T$, the inductor current achieves its minimum value:

$$I_{L,min} = I_{L,max} - \frac{V_s}{L}(1 - d)T \quad (9)$$

define $\Delta i_L = I_{L,max} - I_{L,min}$ as the ripple in the inductor current. From (7) and (9), we deduce:

$$\Delta i_L = \frac{V_e - V_s}{L.f} d \quad (10)$$

$$\Delta i_L = \frac{V_s}{L.f} (1 - d) \quad (11)$$

with $f = 1/T$, switching frequency (Hz).

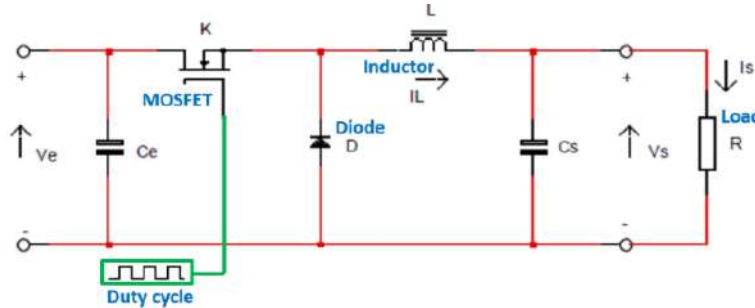


Figure 3. Buck converter

a. Inductor L design

Using (11) and recognizing that the current ripple is maximum at $\alpha = 0.5$, it follows that for a smaller ripple than $\Delta i_{L,max}$. L must be selected as (12).

$$L \geq \frac{V_e}{4\Delta i_{L,max}.f} \quad (12)$$

b. Output voltage ripple V_s , selection of C_s

The capacitor C_s is introduced into the PV system to minimize voltage ripples at the output during the transition of the switch from closed to open and vice versa. In Figure 4, the current i_C flowing through the capacitor C_s is defined as the difference between the current flowing through the inductor and the output current (i_s). The capacitor either stores or releases a charge ΔQ (area of the shaded triangle, with a base of $T/2$ and height $\Delta i_L/2$) this relationship is given by (13) and (14).

$$\Delta Q = T \Delta i_L / 8 \quad (13)$$

$$\Delta Q = C_s \Delta V_s \quad (14)$$

As a result, the capacitance value C_s , enabling a ripple lower than ΔV_s , must adhere to the condition:

$$C_s \geq \frac{\Delta i_L}{8\Delta V_s f} \quad (15)$$

c. Input voltage ripple V_e , selection of C_e

The input voltage ripple ΔV_e is derived from the differential equation that governs the voltage and current in the capacitor C_e (16).

$$\Delta V_s = V_s(T) - V_s(dT) = \frac{1}{C_e} \int_{dT}^T I_e dt \quad (16)$$

$$C_e \geq \frac{I_{PV}}{\Delta V_{smax} f} \quad (17)$$

Based on the equations above and the PV available, Table 3 shows the values of the components used for the buck converter.

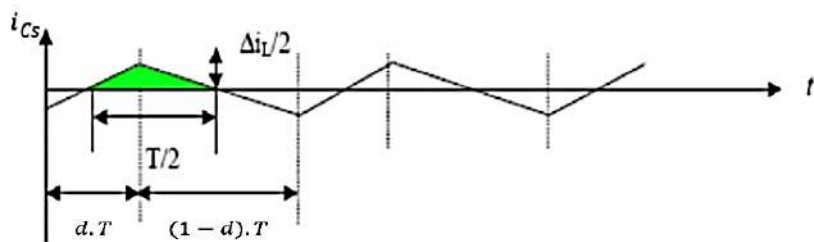


Figure 4. Output capacitor current in a buck converter

Table 3. Parameters of the buck converter for a switching frequency of 8 kHz

Electrical characteristics	Capacitance C_e (μF)	Capacitance C_s (μF)	Resistance R (Ω)	Inductance L (μH)
Value	120	22 μF	2 Ω	470 μH

3. METHODS FOR MPPT

3.1. Suggested MPPT approach

3.1.1. Correlation between optimum current, cell temperature, and solar irradiance

To begin with, we selected two different PV modules, namely: a solar panel POLY-40W and a POLY-30W monocrystalline solar BPSX330J, as described in Table 4. In a subsequent step, using the MATLAB software and its Simulink block diagram, we were able to discern a three-dimensional linear correlation among the optimal current (I_{mpp}), the PV panel temperature (T_{cell}), and solar irradiance (S). Indeed, we investigated the behavior of the I_{mpp} at various temperatures and solar irradiances, as shown in Table 5 for the solar panel POLY-40W and Table 6 for the solar BPSX330J. Subsequently, we plotted this current as a function of temperature and solar irradiance, as depicted in Figure 5 for the solar panel POLY-40W and Figure 6 for the solar BPSX330J. Afterward, we derived (18) through linear regression of three vectors (I_{mpp} [A], T_{cell} [$^{\circ}C$], S [W/m^2]).

$$I_{mpp} = \gamma_0 + \gamma_1 S + \gamma_2 T_{cell} + \gamma_3 S T_{cell} \quad (18)$$

In this equation, γ_0 , γ_1 , γ_2 , and γ_3 are constants specific to the photovoltaic module.

Table 4. Specifications of the POLY-40W and BPSX330J solar panels (S=1000 W/m², AM 1.5, T=25 °C)

Electrical characteristics	Value		Unit
	Solar panel POLY-40W	Solar BPSX330J	
Maximum power P_{mp}	40	30	W
Open circuit voltage (V_{oc})	22	21	V
Voltage at P_{mp} (V_{mp})	18	16.8	V
Temperature coefficient of (V_{oc})	-0.8	-0.8	%/deg. C
Short-circuit current (I_{sc})	2.34	1.94	A
Current at P_{mp} (I_{mp})	2.22	1.78	A
Temperature coefficient of (I_{sc})	0.00247	0.065±0.015	%/°C
Cells per module N_{cell}	36	36	--

Table 5. I_{mpp} as a function of T_{cell} and S for the solar panel POLY-40W PVM

T[°C] S[w/m ²]	0	10	20	30	40	50	60	70
100	0.222	0.221	0.219	0.215	0.212	0.207	0.203	0.194
150	0.335	0.331	0.328	0.326	0.321	0.312	0.305	0.294
200	0.447	0.441	0.439	0.434	0.428	0.418	0.407	0.398
250	0.559	0.555	0.550	0.543	0.533	0.524	0.513	0.498
300	0.671	0.664	0.660	0.658	0.641	0.631	0.620	0.600
350	0.784	0.778	0.775	0.759	0.752	0.737	0.723	0.702
400	0.895	0.886	0.884	0.870	0.858	0.846	0.826	0.808
450	1.008	0.999	0.984	0.982	0.964	0.956	0.927	0.908
500	1.116	1.110	1.103	1.097	1.073	1.055	1.040	1.012
600	1.342	1.336	1.323	1.315	1.293	1.272	1.250	1.219
700	1.572	1.553	1.549	1.527	1.500	1.488	1.452	1.436
800	1.794	1.784	1.753	1.747	1.730	1.710	1.681	1.627
900	2.014	2.006	1.994	1.970	1.958	1.918	1.880	1.838
1000	2.244	2.222	2.219	2.193	2.152	2.130	2.101	2.036

Table 6. I_{mpp} as a function of T_{cell} and S for the solar BPSX330J POLY-30W PVM

T[°C] S[w/m ²]	0	10	20	30	40	50	60	70
100	0.178	0.177	0.178	0.176	0.173	0.171	0.167	0.161
150	0.266	0.266	0.264	0.264	0.262	0.258	0.253	0.244
200	0.357	0.356	0.355	0.353	0.350	0.433	0.340	0.330
250	0.445	0.446	0.444	0.442	0.437	0.433	0.427	0.417
300	0.535	0.535	0.531	0.531	0.528	0.522	0.513	0.503
350	0.625	0.622	0.628	0.621	0.614	0.610	0.599	0.584
400	0.710	0.716	0.712	0.709	0.704	0.696	0.686	0.674
450	0.800	0.802	0.797	0.792	0.792	0.783	0.770	0.756
500	0.895	0.887	0.890	0.883	0.884	0.869	0.860	0.843
600	1.072	1.062	1.070	1.065	1.048	1.045	1.037	1.017
700	1.251	1.249	1.228	1.242	1.239	1.221	1.207	1.182
800	1.421	1.436	1.420	1.418	1.404	1.394	1.372	1.352
900	1.604	1.603	1.607	1.590	1.587	1.563	1.566	1.522
1000	1.787	1.773	1.793	1.777	1.768	1.758	1.730	1.696

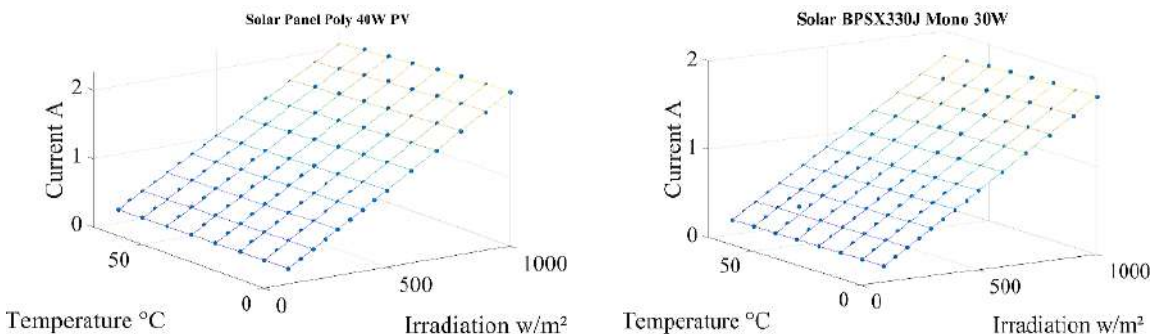
Figure 5. I_{mpp} for the solar panel POLY-40W across a spectrum of S and T_{cell} Figure 6. I_{mpp} for the solar BPS330J-30W across a spectrum of S and T_{cell}

Table 7 displays the coefficient values γ_0 , γ_1 , γ_2 , and γ_3 for the two selected modules. This demonstrates that the R-squared (R^2) is equal to one for both modules, confirming that the coefficients of the linear regression model are accurately inferred. The R^2 value is widely employed in regression analysis [27].

$$R^2 = 1 - \frac{\sum_{k=1}^N (I_{desired} - I_{predicted})^2}{\sum_{k=1}^N (I_{desired} - \bar{I}_{predicted})^2} \quad (19)$$

Where $\bar{I}_{predicted}$ is the arithmetic mean of the predicted current: $\bar{I}_{predicted} = \frac{1}{N} \sum_{k=1}^N I_{predicted}$. Furthermore, it's noteworthy that the coefficient γ_3 remains zero, even with the independence of the selected PVM. As a result, the (20) will be as:

$$I_{mpp} = \gamma_0 + \gamma_1 S + \gamma_2 T_{cell} \quad (20)$$

Table 7. Values obtained for linear regression coefficients

PVM	Type of PVM	γ_0	γ_1	γ_2	γ_3	R^2
Solar BPSX330J	Monocrystalline	0.0006	0.0018	-0.0001	0	0.9992
Solar panel POLY-40W	Polycrystalline	-0.0011	0.00225	-0.0002	0	0.9991

3.1.2. Description of the method TP

Prior to implementing this approach, it is essential to ascertain the linearity coefficients by solving a system of three equations and three unknowns (21) and (22). This procedure must only be carried out once, either automatically by measuring the current corresponding to the three independent MPP per system or manually if the manufacturer supplies these points to users, denoted as $I_{mpp_0}(T_{cell_0}, S_0)$, $I_{mpp_1}(T_{cell_1}, S_1)$, and $I_{mpp_2}(T_{cell_2}, S_2)$.

$$\begin{cases} I_{mpp_0} = \gamma_0 + \gamma_1 S_0 + \gamma_2 T_{cell_0} \\ I_{mpp_1} = \gamma_0 + \gamma_1 S_1 + \gamma_2 T_{cell_1} \\ I_{mpp_2} = \gamma_0 + \gamma_1 S_2 + \gamma_2 T_{cell_2} \end{cases} \Leftrightarrow \begin{pmatrix} I_{mpp_0} \\ I_{mpp_1} \\ I_{mpp_2} \end{pmatrix} = \begin{pmatrix} 1 & S_0 & T_{cell_0} \\ 1 & S_1 & T_{cell_1} \\ 1 & S_2 & T_{cell_2} \end{pmatrix} \begin{pmatrix} \gamma_0 \\ \gamma_1 \\ \gamma_2 \end{pmatrix} \quad (21)$$

Which gives the following linear system:

$$I = B \cdot \gamma \Leftrightarrow \gamma = B^{-1} \cdot I \quad (22)$$

with $I = \begin{pmatrix} I_{mpp_0} \\ I_{mpp_1} \\ I_{mpp_2} \end{pmatrix}$, $B = \begin{pmatrix} 1 & S_0 & T_{cell_0} \\ 1 & S_1 & T_{cell_1} \\ 1 & S_2 & T_{cell_2} \end{pmatrix}$ and $\gamma = \begin{pmatrix} \gamma_0 \\ \gamma_1 \\ \gamma_2 \end{pmatrix}$. Given that these three points of maximum power must adhere to the condition described in (23), ensuring that the matrix B is invertible.

$$S_1 T_{cell_2} + S_2 T_{cell_0} + S_0 T_{cell_1} - (S_1 T_{cell_0} + S_0 T_{cell_2} + S_2 T_{cell_1}) \neq 0 \quad (23)$$

Once the coefficients have been determined, it is possible to directly calculate the optimal current by measuring PV temperature T_{cell} and S, as indicated in (20). This allows continuous and real-time localization of the optimum current by adjusting the duty cycle of the DC-DC converter using the PI controller. We have also introduced a reset button to make our system compatible with other PV panels, which check the specific conditions of our system in terms of power. The algorithm corresponding to the proposed method is presented in Figure 7.

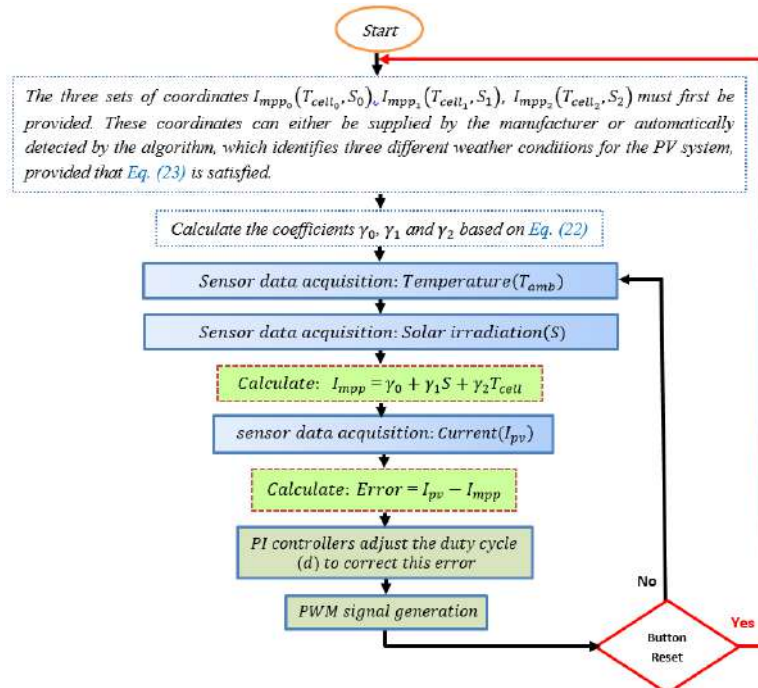


Figure 7. The organization of the new TP in the MPPT of PVS

3.2. Hill climbing

The HC algorithm is commonly utilized to implement MPPT in PVS. The goal of MPPT is to regulate the voltage and current output of a solar panel to keep it at its MPP, where it produces the most energy. The process can be outlined as follows [22]:

- 1) Initialization: start with a specific voltage and current configuration of the solar panel ($d_0 = 0.2$, Step= 1% or 2%).
- 2) Measurement: measure the current power output of the solar panel, denoted as P_i .
- 3) Perturbation: introduce a small perturbation in the voltage or current output while perturbing the duty cycle.

$$d_{i+1} = d_i \pm Step \quad (24)$$

- 4) Measurement: measure the power output again after the perturbation, denoted as P_{i+1} .
- 5) Comparison: compare the new power output with the previous one. If the power has increased $P_{i+1} > P_i$, proceed in the direction of the perturbation. If the power has decreased $P_{i+1} < P_i$, revert to the previous configuration.
- 6) Iteration: repeat steps 3 to 5 iteratively.

3.3. Proposed system: software components

To analyze the performance of the proposed method and the HC method, and to compare them, the software components developed in the MATLAB/Simulink environment are depicted in Figures 8 and 9, corresponding to the new-TP and HC methods, respectively. Both figures share similarities except for block 5, which is introduced in Figure 8 and symbolizes the PI controller with two inputs I_{mpp} and I_{pv} (measured current of the solar panel). This block determines the output duty cycle value required for the coherence of these two currents. The remaining blocks each serve a distinct purpose. Block 1 encompasses the implementation of the MPPT techniques, while block 2 functions as a PWM signal generator operating at a frequency of 8 kHz, dependent on the duty cycles transmitted by block 1 for the HC method and by block 5 for the new-TP method. Blocks 4 and 3 represent the PVG and the buck converter, respectively.

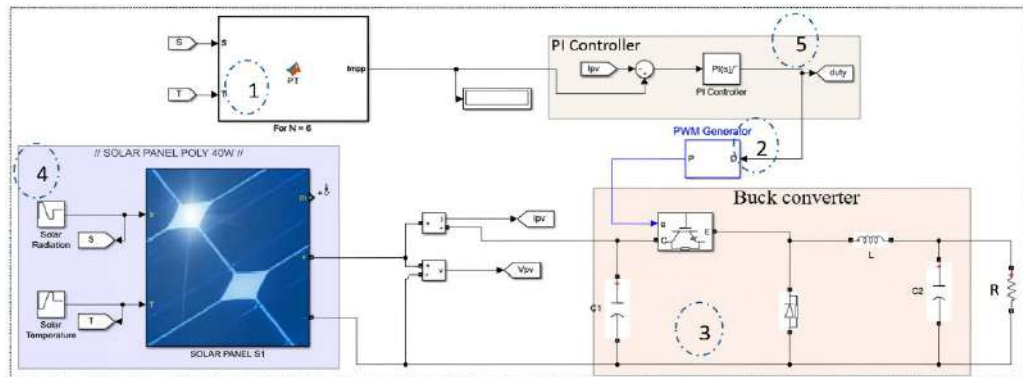


Figure 8. Model of the PVS with PI corrector used for the TP-MPPT method

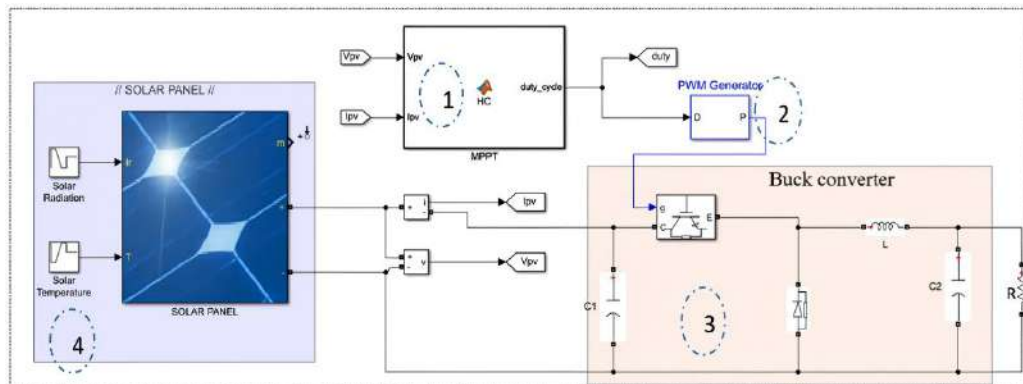


Figure 9. Model of the PVS used for the HC-MPPT method

3.4. Evaluation of techniques

In this work, we have used the criteria presented below to evaluate the superiority of our method compared to the HC method:

- Dynamic response: measures how quickly the MPPT adjusts to changes in sunlight conditions.
- Maximum power efficiency (MPE) [27]: assesses the performance of the MPPT under real operating conditions over an extended period. It gauges the degree of stability, i.e., the MPPT's ability to maintain a stable tracking of the MPP without undesirable oscillations, as well as the efficiency of the utilized system.

$$\text{MPE (\%)} = \frac{\int_0^T P(t) dt}{\int_0^T P_{max}(t) dt} \times 100 \quad (25)$$

Where $P(t)$ is instantaneous real power, $P_{max}(t)$ is maximum theoretical power, and T is the period.

- Adaptability to variable conditions: evaluates the MPPT's capacity to adapt to variations in brightness and temperature.
- Reliability: evaluates the reliability of the MPPT in diverse environments over an extended lifespan.
- Response time ($t_r = t_{(P=P_{max})}$): refers to the time required for the system to reach the solar panel's MPP in the event of changes in environmental or panel characteristics.

3.5. Testing conditions: fixed and dynamic variations in temperature and solar radiation

To showcase the robustness, reliability, and simplicity of our method, we applied it to the two aforementioned solar panels: the solar BPSX330J and the solar panel POLY-40W. The performance of the proposed MPPT algorithm was assessed under both fixed and dynamic temperature and insolation conditions, as illustrated in Figures 10 and 11. The meteorological changes that will affect the PVS can be observed at five points:

- Point 1: ($t_0 = 0$ s): This is the starting point where the temperature T begins at 20 °C and the solar irradiation S starts at 1000 W/m².
- Point 2: ($t_1 = 0.2$ s): There is a dynamic linear increase in temperature to 45 °C, and a dynamic linear decrease in solar irradiation to 500 W/m².
- Point 3: ($t_2 = 0.4$ s): Both the temperature and solar irradiation stabilize at 45 °C and 500 W/m², respectively.
- Point 4: ($t_3 = 0.6$ s): A sudden decrease in temperature to 30 °C occurs, accompanied by a sudden increase in irradiation to 800 W/m², which remains stable until the end of the simulation.

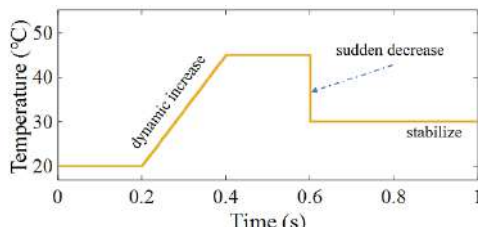


Figure 10. Temperature waveform (T_{cell}) used in the simulation

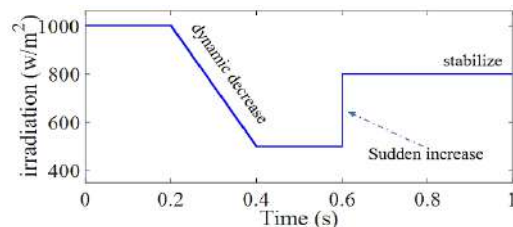


Figure 11. Solar radiation (S) used in the simulation

4. RESULTS AND DISCUSSION

Figures 12 and 13 illustrate the simulation results for the two panels, BPSX330J and POLY-40W, showing the temporal variations of the generated power $P(t)$ in Figures 12(a)-13(a), the buck converter duty cycle $duty(t)$ in Figures 12(c)-13(c), the voltage $V(t)$ in Figures 12(d)-13(d), and the current $I(t)$ in Figures 12(b)-13(b) for both methods. The total simulation time is set to one second. The system performance measurements are detailed in Table 8. The results of our method were then compared to those obtained with the HC method with perturbation steps of 1% and 2%. This comparative analysis allowed us to emphasize the efficiency of MPE, speed (t_c), and stabilization capabilities of our algorithm in contrast to the steady-state oscillations observed in the HC algorithm.

TP_new demonstrated the ability to attain the MPP with a convergence time of approximately 0.01 s for the solar BPSX330J and about 0.008 s for the panel POLY-40W, accompanied by minimal oscillations around the MPP. In contrast, the HC method required 0.193 s to reach the maximum power with a

disturbance step of 1% and approximately 0.1 s with a step of 2% for the solar BPSX330J. For the solar panel POLY-40W, HC took 0.194 s for a step of 1% and roughly 0.104 s for a step of 2%. On average, the convergence times were 0.009 s for TP_new, 0.1935 s for HC (1%), and 0.102 s for HC (2%). This shows that our method offers superior convergence speed, with a significant reduction in convergence time of 95.348% compared to HC (1%) and 91.176% compared to HC (2%). This result is visible in Figure 12(c) and Figure 13(c), which show that the duty cycle of the proposed method quickly detects the PPM, while the duty cycle of the HC method takes more time to reach the PPM. Notably, HC exhibited more pronounced oscillations with an increase in disturbance step, while our method demonstrated almost weak oscillations.

To better understand the accuracy and reliability of the model, we performed a thorough MPE analysis to measure the accumulated captured energy. The results show that the TP method achieves the highest MPE values for both PV panels, with an average MPE of 98.18% for TP, 90.065% for HC (1%), and 83.615% for HC (2%). This represents a significant increase in captured energy of 8.265% compared to HC (1%) and 14.83% compared to HC (2%). These results suggest that using a tracker based on TP-new places a strong emphasis on the speed of reaching the MPP, compared to HC-based trackers, as well as on energy accumulation under various test conditions. This allows it to be experimentally implemented on different types of boards, thanks to simple calculations and low memory requirements, making it a promising solution for the future.

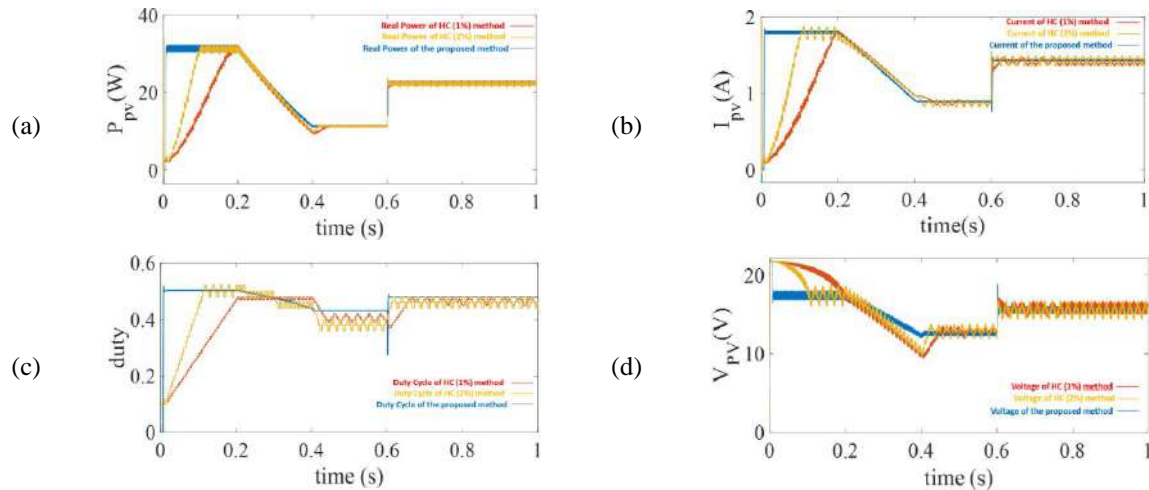


Figure 12. Simulation results for BPSX330J for TP and HC 1% and 2%: (a) power at the PV output $P_{pv}(t)$, (b) current $I_{pv}(t)$, (c) $duty(t)$, and (d) voltage $V_{pv}(t)$

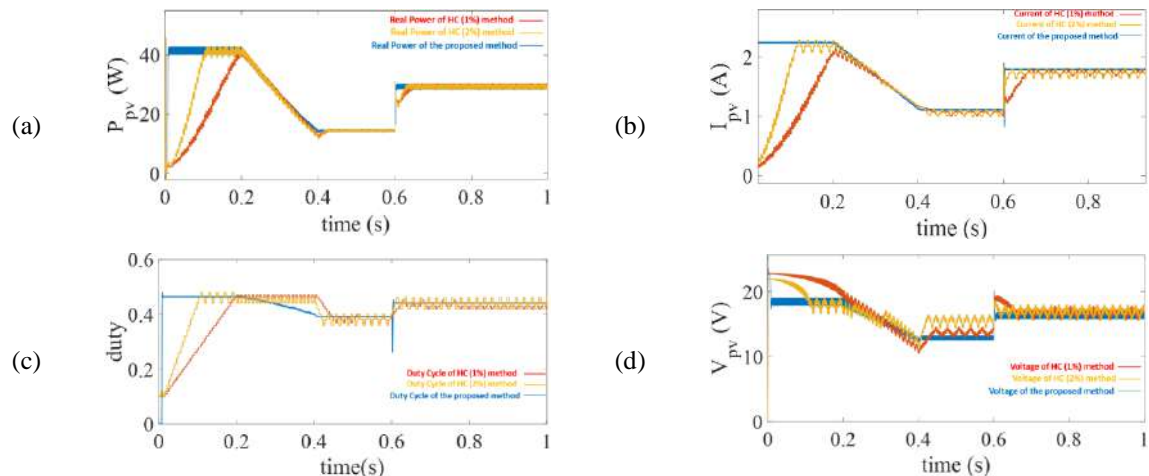


Figure 13. Simulation results for the 40 W solar panel for TP and HC 1% and 2%: (a) power at the PV output $P_{pv}(t)$, (b) current $I_{pv}(t)$, (c) $duty(t)$, and (d) voltage $V_{pv}(t)$

Table 8. Full simulation analysis of HC and TP-MPPT methods applied to different types of PVM

Type of PVM	Strategy	Oscillation		Initial	MPE (%)	
		<i>I(A)</i>	<i>V(V)</i>	<i>Duty</i>	<i>t_c(s)</i>	
Solar panel BPSX330J	New-TP	Weak	Weak	Weak	0.010	97.96
	HC (1%)	Medium	Medium	Medium	0.193	90.43
	HC (2%)	Strong	Strong	Strong	0.100	84.11
Solar panel POLY-40W	New-TP	Weak	Weak	Weak	0.008	98.40
	HC (1%)	Medium	Medium	Medium	0.194	89.70
	HC (2%)	Strong	Strong	Strong	0.104	83.12
		Average		New-PT	0.009	98.18
		Average		HC 1%	0.1935	90.065
		Average		HC 2%	0.102	83.615

5. CONCLUSION

This work aims to introduce, model, and design the innovative New-TP approach as an MPPT technique for capturing MPP in PVS under different weather conditions. The core concept of this method involves establishing a linear correlation among three parameters (T_{cell} , S , and I_{mpp}). Once identified, this correlation enables real-time prediction and monitoring of the MPP, even in fluctuating conditions. Simulation was carried out using the MATLAB Simulink environment, incorporating a buck converter with a PI controller. Comparative analyses were performed using the HC method for two disturbance levels (1% and 2%), considering two distinct panels, the solar BPSX330J and the solar POLY-40W, in fixed and dynamic environmental scenarios. The TP-new algorithm outperformed the HC algorithm under all tested conditions, demonstrating superior performance. The controller's tracking time was significantly reduced by 90%, resulting in an average convergence time of 0.009 s. Regarding oscillation, the TP algorithm exhibited the smallest fluctuations around the MPP with the highest MPE of 98.18%, leading to improved efficiency and a substantial increase in harvested energy. This comparison highlights the advantages of our method in terms of faster convergence and enhanced efficiency.

FUNDING INFORMATION

Authors state no funding involved.

AUTHOR CONTRIBUTIONS STATEMENT

This journal uses the Contributor Roles Taxonomy (CRediT) to recognize individual author contributions, reduce authorship disputes, and facilitate collaboration.

Name of Author	C	M	So	Va	Fo	I	R	D	O	E	Vi	Su	P	Fu
Soufyane Ait El Ouahab	✓	✓	✓	✓	✓	✓	✓	✓	✓	✓	✓	✓	✓	✓
Firdaous Bakkali				✓	✓					✓				
Abdellah Amghar		✓		✓	✓	✓			✓		✓	✓	✓	✓
Rachid Zriouile				✓	✓				✓					
Hassan Sahsah				✓	✓				✓					✓
Meriem Boudouane				✓	✓				✓					

C : Conceptualization

M : Methodology

So : Software

Va : Validation

Fo : Formal analysis

I : Investigation

R : Resources

D : Data Curation

O : Writing - Original Draft

E : Writing - Review & Editing

Vi : Visualization

Su : Supervision

P : Project administration

Fu : Funding acquisition

CONFLICT OF INTEREST STATEMENT

Authors state no conflict of interest.

DATA AVAILABILITY

The authors confirm that the data supporting the findings of this study are available within the article [and/or its supplementary materials].

REFERENCES

- [1] G. Mestrallet, "The formidable challenge of energy production in a radically changing world (in French: Le formidable défi de la production d'énergie dans un monde en profonde évolution)," *Annales des Mines - Responsabilité et environnement*, vol. N° 78, no. 2, pp. 24–28, May 2015, doi: 10.3917/re1.078.0024.
- [2] P. Meenalochini, P. R. A., R. Pugalenth, and J. A., "Energy management of grid connected PV with efficient inverter based wireless electric vehicle battery charger: A hybrid CSA-QNN technique," *Journal of Energy Storage*, vol. 80, p. 110255, Mar. 2024, doi: 10.1016/j.est.2023.110255.
- [3] P. Upadhyay and R. Kumar, "A ZVS-ZCS quadratic boost converter to utilize the energy of PV irrigation system for electric vehicle charging application," *Solar Energy*, vol. 206, pp. 106–119, Aug. 2020, doi: 10.1016/j.solener.2020.05.068.
- [4] B. Chwieduk and D. Chwieduk, "Analysis of operation and energy performance of a heat pump driven by a PV system for space heating of a single family house in polish conditions," *Renewable Energy*, vol. 165, pp. 117–126, Mar. 2021, doi: 10.1016/j.renene.2020.11.026.
- [5] S. Amose Dinakaran, A. Bhuvanesh, A. S. Kamaraja, P. Anitha, K. Karthik Kumar, and P. Nirmal Kumar, "Modelling and performance analysis of improved incremental conductance MPPT technique for water pumping system," *Measurement: Sensors*, vol. 30, p. 100895, Dec. 2023, doi: 10.1016/j.measen.2023.100895.
- [6] S. Manna *et al.*, "Design and implementation of a new adaptive MPPT controller for solar PV systems," *Energy Reports*, vol. 9, pp. 1818–1829, Dec. 2023, doi: 10.1016/j.egyr.2022.12.152.
- [7] S. A. E. Ouahab, F. Bakkali, A. Amghar, H. Sahsah, L. Mentaly, and L. Mahfoud, "Design and implementation of temperature-parametric for maximum power point tracking of photovoltaic systems: Experimental validation using PI controller," *Computers and Electrical Engineering*, vol. 120, p. 109707, Dec. 2024, doi: 10.1016/j.compeleceng.2024.109707.
- [8] A. Refaat, A.-E. Khalifa, M. M. Elsakka, Y. Elhenawy, A. Kalas, and M. H. Elfar, "A novel metaheuristic MPPT technique based on enhanced autonomous group particle swarm optimization algorithm to track the GMPP under partial shading conditions - Experimental validation," *Energy Conversion and Management*, vol. 287, p. 117124, Jul. 2023, doi: 10.1016/j.enconman.2023.117124.
- [9] A. F. Sagonda and K. A. Folly, "A comparative study between deterministic and two meta-heuristic algorithms for solar PV MPPT control under partial shading conditions," *Systems and Soft Computing*, vol. 4, p. 200040, Dec. 2022, doi: 10.1016/j.sasc.2022.200040.
- [10] L. Gong, G. Hou, and C. Huang, "A two-stage MPPT controller for PV system based on the improved artificial bee colony and simultaneous heat transfer search algorithm," *ISA Transactions*, vol. 132, pp. 428–443, 2023, doi: 10.1016/j.isatra.2022.06.005.
- [11] S. K. T., V. Reddy, and A. Robinson, "An innovative grey wolf optimizer with Nelder–mead search method based MPPT technique for fast convergence under partial shading conditions," *Sustainable Energy Technologies and Assessments*, vol. 59, p. 103412, Oct. 2023, doi: 10.1016/j.seta.2023.103412.
- [12] M. Agdam *et al.*, "A novel algorithm MPPT controller based on the herd horse optimization for photovoltaic systems under partial shadow conditions," *Engineering Research Express*, vol. 6, no. 3, 2024, doi: 10.1088/2631-8695/ad5f16.
- [13] A. A. Zaki Diab and H. Rezk, "Global MPPT based on flower pollination and differential evolution algorithms to mitigate partial shading in building integrated PV system," *Solar Energy*, vol. 157, pp. 171–186, Nov. 2017, doi: 10.1016/j.solener.2017.08.024.
- [14] M. I. Mosaad, M. O. Abed el-Raouf, M. A. Al-Ahmar, and F. A. Banakher, "Maximum power point tracking of PV system based cuckoo search algorithm; review and comparison," *Energy Procedia*, vol. 162, pp. 117–126, Apr. 2019, doi: 10.1016/j.egypro.2019.04.013.
- [15] S. A. El Ouahab, F. Bakkali, A. Amghar, H. Sahsah, L. El Mentaly, and M. Boudouane, "Bonobo optimizer: dynamically adaptive heuristic for enhanced MPPT in photovoltaic systems under partial shading – experimental validation with buck converter," *International Journal of Emerging Electric Power Systems*, Dec. 2024, doi: 10.1515/ijeeps-2024-0193.
- [16] M. Park and I.-K. Yu, "A study on the optimal voltage for MPPT obtained by surface temperature of solar cell," in *30th Annual Conference of IEEE Industrial Electronics Society, 2004. IECON 2004*, vol. 3, pp. 2040–2045, doi: 10.1109/IECON.2004.1432110.
- [17] L. El Mentaly, A. Amghar, and H. Sahsah, "Improvement of the temperature parametric (TP) method for fast tracking of maximum power point in photovoltaic modules," *International Journal of Emerging Electric Power Systems*, vol. 20, no. 5, Oct. 2019, doi: 10.1515/ijeeps-2018-0311.
- [18] L. El Mentaly, A. Amghar, and H. Sahsah, "The prediction of the maximum power of PV modules associated with a static converter under different environmental conditions," *Materials Today: Proceedings*, vol. 24, pp. 125–129, 2020, doi: 10.1016/j.matpr.2019.07.704.
- [19] A. Hassan, O. Bass, and M. A. S. Masoum, "An improved genetic algorithm based fractional open circuit voltage MPPT for solar PV systems," *Energy Reports*, vol. 9, pp. 1535–1548, 2023, doi: 10.1016/j.egyr.2022.12.088.
- [20] A. Satif, L. Hlou, M. Benbrahim, H. Erguig, and R. Elgouri, "Simulation and analysis of A PV system with P and O MPPT algorithm using A PI controller for buck converter," *ARPN Journal of Engineering and Applied Sciences*, vol. 13, no. 9, pp. 3014–3022, 2018.
- [21] D. B. Hmamou *et al.*, "A novel hybrid numerical with analytical approach for parameter extraction of photovoltaic modules," *Energy Conversion and Management: X*, vol. 14, p. 100219, May 2022, doi: 10.1016/j.ecmx.2022.100219.
- [22] L. El Mentaly, A. Amghar, and H. Sahsah, "Comparison between HC, FOCV and TG MPPT algorithms for PV solar systems using buck converter," in *2017 International Conference on Wireless Technologies, Embedded and Intelligent Systems (WITS)*, Apr. 2017, pp. 1–5, doi: 10.1109/WITS.2017.7934609.
- [23] G. Mustafa, F. Ahmad, R. Zhang, E. U. Haq, and M. Hussain, "Adaptive sliding mode control of buck converter feeding resistive and constant power load in DC microgrid," *Energy Reports*, vol. 9, pp. 1026–1035, Mar. 2023, doi: 10.1016/j.egyr.2022.11.131.
- [24] J. López, S. I. Sename, P. F. Donoso, L. M. F. Morais, P. C. Cortizo, and M. A. Severo, "Digital control strategy for a buck converter operating as a battery charger for stand-alone photovoltaic systems," *Solar Energy*, vol. 140, pp. 171–187, Dec. 2016, doi: 10.1016/j.solener.2016.11.005.
- [25] R. Ayop, M. F. I. Zaki, C. W. Tan, S. Md Ayob, and M. J. Abdul Aziz, "Optimum sizing of components for photovoltaic maximum power point tracking buck converter," *Solar Energy*, vol. 243, pp. 236–246, Sep. 2022, doi: 10.1016/j.solener.2022.07.032.
- [26] A. Emadi, A. Khaligh, Z. Nie, and Y. Joo Lee, *Integrated power electronic converters and digital control*. CRC Press, 2017. doi: 10.1201/9781439800706.
- [27] D. B. Hmamou *et al.*, "Experimental characterization of photovoltaic systems using sensors based on MicroLab card: design, implementation, and modeling," *Renewable Energy*, vol. 223, p. 120049, Mar. 2024, doi: 10.1016/j.renene.2024.120049.

APPENDIX

Table 1. A review of studies in the literature that use the correlation between different parameters

Ref.	Decision variable	Equation, discussion, remarks, and results
[16]	PI corrector V_{mpp}	<ul style="list-style-type: none"> - In this paper, the authors formulated a linearized equation model based on a polycrystalline PV panel, characterizing the optimal voltage (V_{mpp}) in relation to T_{cell} and solar irradiation (S). $V_{mpp} \cong (u + S \cdot v) - T_{cell} (w + S \cdot y) \quad (1)$ <ul style="list-style-type: none"> - The parameters u, v, w, and y vary depending on the sunlight level. The authors partitioned the sunlight range [100; 1000] W/m^2 into nine intervals, assigning unique values to each interval. - The main drawback is that PV modules (PVM) exhibit differing optimal voltages under identical temperature and solar radiation conditions.
[17]	Duty cycle $d = \frac{V_{out}}{V_{mpp}}$ Where V_{out} : voltage at buck converter output	<ul style="list-style-type: none"> - In this investigation, the researchers utilized MATLAB to generate three-dimensional plots (S, ambient temperature (T_{amb}) and V_{mpp} within the temperature range [0; 90] °C and solar irradiance range [50; 1000] W/m^2 for three distinct PVM: MSX-60 Poly, FS-265 Thin Film CdS/CdTe, and Sun E19320 Mono. - They proposed a 3D linear model expressed by the relation: $V_{mpp} = \gamma_0 + \gamma_1 S + \gamma_2 T_{amb} \quad (2)$ <p>where γ_0, γ_1, and γ_2 are parameters specific to the PV model. The linearity of this model is affirmed by an R-squared (R^2) value of 0.9793 for MSX-60, 0.8816 for FS-265, and 0.9675 for E19320.</p> <ul style="list-style-type: none"> - A simulation study was conducted in the PSIM environment, involving a buck converter, a battery, and the three aforementioned PVM types. The authors compared their proposed method with the HC method. - Results indicate the superiority of the proposed method in terms of rapid convergence and effective tracking in dynamically changing conditions. - The authors introduced a novel approach for predicting the maximum power output of a PV panel.
[18]	-	$P_{mpp} = \gamma_0 + \gamma_1 S + \gamma_2 T_{amb} + \gamma_3 S T_{amb} \quad (3)$ <p>Where γ_0, γ_1, γ_2, and γ_3 are parameters specific to the PV model.</p> <p>This technique is not implemented as an MPPT algorithm. Instead, its purpose is to assess the efficiency of MPPT methods employed in converters, evaluating their ability to track the MPP.</p> <ul style="list-style-type: none"> - Simulation results conducted in the PSIM environment demonstrated that the proposed model yielded favorable outcomes, particularly when applied to Kyocera's KD215GX polycrystalline module, achieving a regression coefficient R^2 of 0.9702 and an MPPT efficiency of the HC algorithm at 97%.
Proposed TP	PI corrector I_{mpp}	<p>This research introduces a novel approach to temperature parametric for the prompt identification and tracking of the MPP. It involves establishing a 3D linear correlation among the current corresponding to the MPP (I_{mpp}), S, and T_{cell}. A simulation study was conducted in the MATLAB-Simulink environment to assess the efficacy of the proposed method. The evaluation was performed on two types of PV panels, namely solar BPSX330J and POLY-40W, under fixed and dynamic environmental conditions. A comparison was made with the HC using two increment steps, 1% and 2%. The simulation results consistently indicate that the proposed TP outperforms the HC in terms of MPP detection. It features faster convergence time 0.009 s and an MPPT efficiency at 98.18%, reduced steady-state oscillations, and superior sensing performance for both types of PV panels.</p>

BIOGRAPHIES OF AUTHORS



Soufyane Ait El Ouahab received his Lic. degree in Electronics and Systems of Communication from Ibn Zohr University. Hold a Master's degree in Systems and Telecommunication from the Faculty of Sciences, Ibn Zohr University, Agadir, Morocco. Currently, a Ph.D. student in Electronics and Renewable Energies at the Department of Physics, Laboratory of Metrology and Information Processing Lab, Ibn Zohr University. His main research interests include contribution to the improvement of MPPT techniques associated with a set of PV generators under shade. He can be contacted at email: soufyane.aitelouahab@edu.uiz.ac.ma.



Firdaous Bakkali is currently working as a lecturer at the Faculty of Sciences (Department of Physics) at Ibn Zohr University - Agadir. She is conducting research in measurement science and technology. She can be contacted at email: f.bakkali@gmail.com.



Abdellah Amghar currently works at the Physics, Ibn Zohr University - Agadir. Amghar does research in materials physics, instrumentation engineering, and computer engineering. Their current project is 'MPPT controllers'. He can be contacted at email: a.amghar@uiz.ac.ma.



Rachid Zriouile was born in Agadir, Morocco, in 1992. In 2012, he obtained a University Diploma in Technology, option Electrical Engineering, from the High School of Technology in Agadir. In 2015, he got an engineering diploma in Electrotechnics and Industrial Electronics from the Faculty of Sciences and Techniques of Beni Mellal. His research focuses on renewable energy. Currently, he is working on his doctoral thesis titled "Energy optimization of a system based on renewable energies and management of its integration into the electrical grid". He can be contacted at email: rachid.zriouile@edu.uiz.ac.ma.



Hassan Sahsah is currently a Professor at Faculty of Sciences, Department of Physics, Ibn Zohr University in Agadir. He obtained his Ph.D. degree in Opto-Electronics and Instrumentation from Jean Monnet University, Faculty of Sciences-Saint Etienne, in 1994. His research interest includes photovoltaic system and opto-electronics. He can be contacted at email: h.sahsah@uiz.ac.ma.



Meriem Boudouane graduated in Electronics from Al Idrissi Technical High School. She then obtained a University Diploma of Technology (DUT) in Electrical Engineering from the Higher School of Technology (EST) Agadir, a fundamental degree in Physical Sciences, and a Master's degree in Materials Engineering and Renewable Energy at the Physics Department of the Faculty of Science, University Ibn Zohr Agadir, Morocco. She is currently working on her research into the management and optimization of microgrid energy flows. She can be contacted at email: meriemprof@gmail.com.